Geology, Master Of Science
École Normale Supérieure de Lyon
Université Claude Bernard Lyon I

Internship 2016 – 2017
Romain Caneill
M2 géologie

Internship under the guidance of Ghislain Picard [1]

Analysis of Elevation Maps Measured by Laser Scannering at Dome C, Antarctica. Investigation of Snow Accumulation Processes.

Abstract: *Antarctica is largely covered by sastrugi fields, elongated erosion structures oriented along the main direction of wind. These shapes influence albedo, heat transfers, and thus the energy balance of the continent.*
A laser scanner is installed at Dome C, on the Antarctic Plateau, since 2015. It provides almost daily elevation maps of an area which surface is about 100 m^2. These unrivaled data bring new informations about the 3D structure of the surface. During my internship I developed new tools adapted to elevation maps in Antarctica like accumulation maps, detection of deposit patches through segmentation, and deposit age maps. The first step to compute aerodynamic roughness as a function of the orientation has been computed with the help of scripts developed for another scanner placed in the French Alps.
The annual mean accumulation is few centimeter at Dome C but this small elevation hides complex deposit and erosion processes, with common snow drift. About half of the accumulation maps present patches associated with erosion. Some events present well oriented patches along wind direction but this behavior is not systematic. The patches are also detectable on the surface deposit age maps. As during one event snow is deposited in patches, surface deposit age is not reinitialized everywhere. Erosion helps also to create heterogeneous deposit age maps and erosion mainly occurs at the same time as deposit events. Thus the exposition time of the surface should not be considered as homogeneous.
Further work is necessary to study more precisely data from the laser scanner but it is now clear that the mean accumulation is not sufficient to describe the evolution of the surface. Snow drift and erosion are major part of numerous events and constantly renew the surface shape.

Keywords: *Rugged Laser Scan, Snow accumulation, Antarctica, Sastrugi*

[1] ghislain.picard@univ-grenoble-alpes.fr
Institut des Géosciences de l'Environnement
54, rue Molière
38 400 Saint Martin d'Hères
http://www.ige-grenoble.fr/

Acknowledgements

I gratefully thank Ghislain Picard for supervising my internship. His advices were useful to the progress of my research. The data he gave me were directly usable and thanks to that I was able to rapidly start the research without loosing too much time in data processing. His knowledge of Antarctica field and his intuitions were helpful to choose the direction of my work.

Étienne Vignon helped me a lot on the understanding of aerodynamic processes near the surface. I thank him for the time he spent at the beginning of my internship when Ghislain was still on field work in Antarctica. His ideas about surface shapes and his vision of wind were helpful for my roughness computations.

I thank Florence Naaim and Hervé Bellot from IRSTEA laboratory for the explications they gave me on the RLS placed on Alps and on sastrugi, for the field mission on the meteorological station placed at Col du Lac Blanc (French Alps), and for the advices they gave me about my work. I also thank Hervé for giving me his aerodynamic scripts and for the explication of how they work.

I thank Christophe Genthon for the access of Dome C meteorological data, Laurent Arnaud for his advices and all the LGGE research team for their warm reception.

Contents

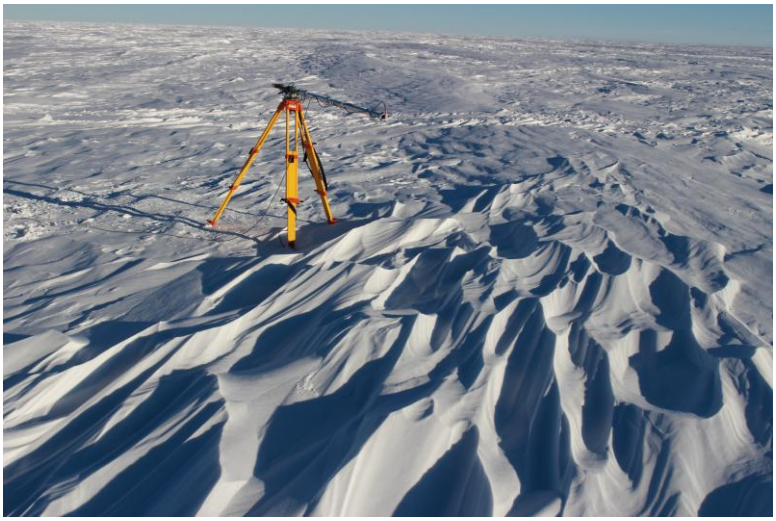

Figure 1: Sastrugi field in Antarctica. Credits Ghislain Picard.

1 Introduction

Antarctica contains 70% of world fresh water and if all Antarctica melts, sea level would rise by 58 m. As Antarctica is the coldest continent on Earth, the hypothesis of a total melt is not realistic for the near future. Nevertheless on average its contribution on global level rise is uncertain and will probably increase in current century (*Shepherd and Wingham*, 2007).

The energy balance, which is influenced by surface properties (*Brun et al.*, 2011), is an important quantity to forecast the future climate of this region. The amount of energy absorbed by the surface is controlled by the snow albedo. The albedo is largely influenced by small sized snow grain deposed on surface (*Picard et al.*, 2012), by the snow metamorphism, by hoar crystal and by the surface physical roughness (*Zhuravleva and Kokhanovsky*, 2011).

A large part of Antarctica is covered by elongated shapes called sastrugi (Figure 1). Sastrugi are erosional forms created by wind and oriented along its prevailing direction (*Filhol and Sturm*, 2015). When the wind blows perpendicularly to the sastrugi, this causes an increasing of aerodynamic roughness (*Jackson and Carroll*, 1978; *Vignon et al.*, 2016) and thus of turbulence. The increasing of turbulence kinetic energy is sufficient to destruct hoar crystals (*Champollion et al.*, 2013) and thus influence the snow albedo. As the aerodynamic roughness is linked to physical roughness (*Lettau*, 1969), the shape of the surface plays a role on the energy balance of the continent.

In the coastal environment of Antarctica, where temperature is higher and where precipitations are higher than in the Antarctic Plateau, sastrugi can reorient themselves in direction of predominant wind (*Amory et al.*, 2016). An effect of this reorientation is the decreasing of aerodynamic roughness along the wind direction. On the Antarctic Plateau, accumulation is driven by wind (*Libois et al.*, 2014; *Groot Zwaaftink et al.*, 2013), on the contrary of the Alps. In the Alps some big snowfalls occur during the winter, adding few decimeter of snow to the surface and sometimes reseting its carved shapes to a smooth and regular surface. Instead of this metric year accumulation, only 8 centimeter are deposited on surface each year at Dome C (*Picard et al.*, 2016). In contrast with the small mean accumulation, a lot of snow is eroded and drifted, creating deposit patches that are visible on the field or photographs. Accumulation processes are different in the Alps and in Antarctica and the methods to study them are not the same.

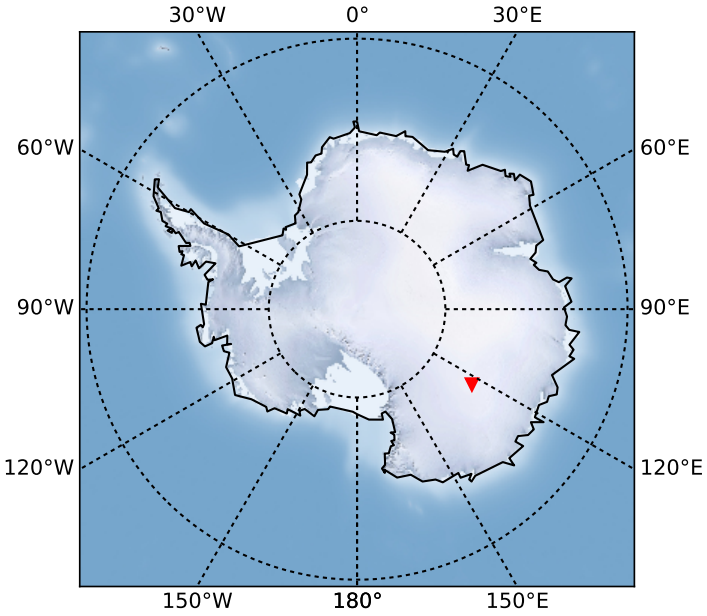

Figure 2: Map of Antarctica with Dome C (red triangle).

Dome C is situated in the Antarctic Plateau, (75°06' S, 123°20' E), 3200 m above sea level. Figure 2 shows a map of Antarctica, the red triangle represents Dome C. Figure 3 presents the annual wind rose at Dome C. Wind is mainly oriented along north – south axis and is usually under $5\,\mathrm{m\,s^{-1}}$.

A laser scanner is installed at Dome C since 2015, providing almost daily elevation maps of surface. These unrivaled data have not been deeply studied before my internship and lot of hope is placed on the potential of this instrument. Other studies using laser scanner exist on snow (*Schirmer et al.*, 2011; *Lacroix et al.*, 2008; *Kaasalainen et al.*, 2011; *Kukko et al.*, 2013) but they are not effectuated at Dome C and thus the accumulation study tools and methods are not fully adapted here. In addition, only with a fixed laser scanner temporal evolution of surface has not been studied. Elevation maps can provide tools to understand snow drift that is important for snowpack model Crocus (*Libois et al.*, 2014) and accurate dating ice cores with water isotopes (*Ding et al.*, 2017). The aim of my internship was to study elevation maps, create new tools and algorithms adapted to the laser scanner, explore accumulation processes, and start the study of exposition time, important in all the air – snow exchange processes.

I analyzed observation data from a Rugged Laser Scan. All the processing were done with the Python programing language. The following list resumes the work I effectuated on the data:

- I worked on gridded data, processes described on Section 2.2 have been already implemented and computed by the research team which hosted me. Resulting elevation maps were almost clean, only some perturbations due to shrouds persisted. I removed some aberrant values that were too elevated. I spent time on studying the different events and their effects on elevation.

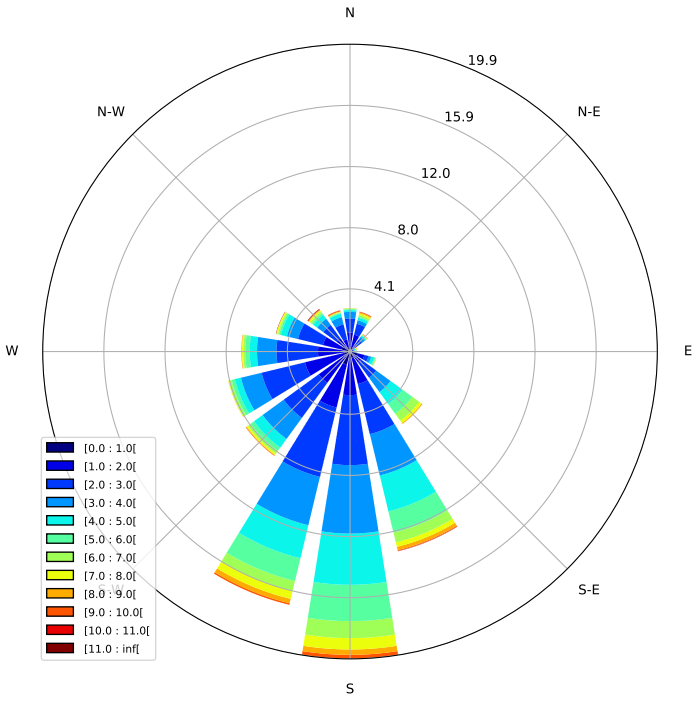

Figure 3: Annual wind rose at Dome C. The bars represent the direction where the wind is coming from and the colors represent wind speed in $\mathrm{m\,s^{-1}}$. The measurements have been taken at 2.5 m height.

- With the help of bibliography I tried some metrics to help the comprehension of accumulation processes. Metrics that characterize physical roughness and its orientation were used but many of them did not give any significant results. The elevation root mean square (RMS) is sufficient to my applications.
- Aerodynamic silhouette area was computed with existing scripts written by Hervé Bellot for a RLS placed on Alps, this RLS is described by *Picard et al.* (2016). The work I did was to process them with data from the RLS placed at Dome C.
- I created my own analyze scripts with the help of my supervisor's advices. We designed an algorithm to compute deposit age, I implemented it, as well as accumulation maps and patches segmentation with the python library *skimage*. I tried different thresholds in these scripts to find the better ones.

This report is divided on four part. I will present the materials and the methods I used during my internship to study accumulation processes. Next section will show results we found, followed by a discussion of methods and results. Last section will conclude with a summary of results and possible following works.

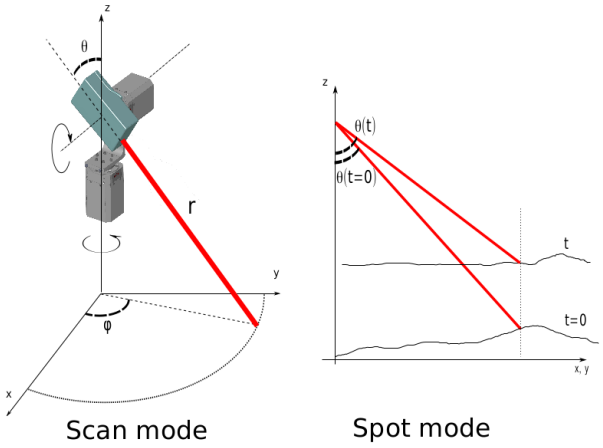

Figure 4: Principle of the Rugged Laser Scan (RLS): zenith angle θ and azimuth angle ϕ control the point where the telemeter is pointing. Figure from *Picard et al.* (2016).

2 Materials and methods

2.1 Rugged Laser Scan (RLS)

Picard et al. (2016) developed a laser scan able to resist to the very harsh conditions that occur at Dome C, Antarctica, where temperature usually falls under $-70°C$ and wind can exceed $10\,m\,s^{-1}$. The RLS have been installed from January 2015 to January 2016 3 meters over the surface and have been risen up to 4.5 m in February 2016 to scan a larger surface. The two datasets have been respectively named *dmc1* and *dmc2*. The RLS is programmed to acquire one scan per day, but unfortunately during big snow drifting events the acquisitions do not work, because the telemeter detects some of the transported particles instead of the ground. This effect, added to some technical problems, decreases the number of valid scans to 511 during the two years of acquisitions: the success rate is 65% for *dmc1* and 72% for *dmc2*.

Figure 4 presents the working principle of the RLS: an industrial laser meter mounted on two motors placed perpendicularly. These two motors allow two rotation axis in the zenith and azimuth directions: the telemeter can point anywhere in the surface. The RLS acquires about $2 \cdot 10^5$ points in four hours, with a precision of 1 cm and an accuracy of 5 cm or better. This corresponds to a surface of about 120 m^2 for the *dmc2* dataset.

2.2 Acquisition and elevation maps processing

To minimize the perturbation on the wind, the RLS is mounted on a thin structure (38 mm diameter). Shrouds maintain the mast vertically, minimizing oscillations. During the installation, polystyrene spheres have been installed in the scanned field and leveled to a horizontal plane. A post acquisition processing can be used to verify the stability of the structure and calibrate the transformation to level the scan. Figure 5 shows a photograph of the RLS, corresponding to *dmc2* settings. The RLS is at the top of the mast in the black box. The four calibrating sphere are visible in the snow surface.

RLS has been used on *scan mode* to detect accumulation and patches. During the scanning process, the RLS scans ϕ from -90 to 90 degrees and θ from 19 to 62 degrees. The increments $\Delta\phi$ and $\Delta\theta$ are adjusted with θ to create a uniform spatial resolution on the surface.

The raw output data are expressed in spherical coordinates. To deduce Cartesian coordinates that are more adapted, some steps are necessary. A cleaning is also applied during this

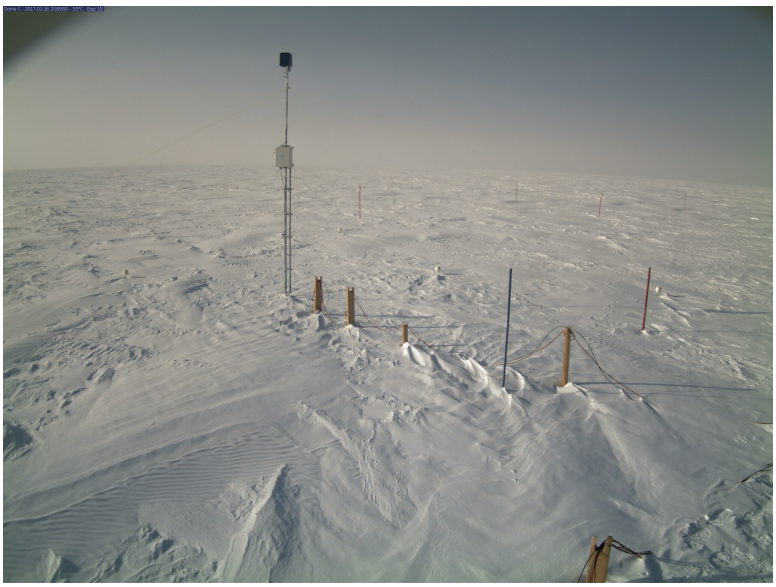

Figure 5: Photograph showing the RLS mounted on top of the mast, the calibrating spheres and the scanned snow surface. Credits Ghislain Picard.

processing:

1. The telemeter has an internal software that returns measurement only when the quality is estimated to be sufficient enough.
2. The elevation data are projected in the (x, y, z) coordinate system.
3. The rotation is applied to the dataset to ensure the horizontal orientation of the plane (x, y)
4. A filter is applied to remove outliers: any point more than 5 cm away from the neighbourhood's mean is removed. The neighbourhood is chosen as a circus of radius 5 cm centered on the tested point. During this step the spheres are also removed.
5. Finally a bilinear interpolation on a regular grid is computed. The same grid is used for all the scans of the same dataset *dmc1* or *dmc2*.

Too high values around position of shrouds were removed with a script that considers every position over 40 cm is too high. This was sufficient to remove the main aberrant values.

All elevation maps do not have exactly the same borders. Different causes can be responsible of these variations: when RLS zenith angle variations does not reach its maximum or minimum value or when border values are removed by the RLS internal software. A mask is applied to remove the borders so every elevation maps have the same surface. After this step, the scans surface is equal to 94.5 m^2 for *dmc2*.

To determinate the orientation of the RLS, we used the shadow of the mast and the calibration spheres. A camera takes hourly photographs of the scanned field. When the shadow of the RLS passes over one sphere it is possible to calculate the azimuth of the sun and thus orientation of the spheres on the scan. Orientation of x-axis is then derived. A value of 116 °N has been calculated, with an uncertainty under 15 °. This angle corresponds to movement of the sun during one hour, which is the temporal resolution of the photographs. The south direction is represented with a black arrow on maps.

2.3 Derivation of aerodynamic roughness from elevation maps

Lettau (1969) proposed a simple formula to estimate aerodynamic roughness from easily measurable parameters:

$$z_0 = 0.5h^* \frac{s}{S} \tag{1}$$

where z^* is the effective obstacle height in cm. A value of two standard deviation of the elevation distribution is usually taken (*Brock et al.*, 2006). s is the silhouette area which corresponds to the surface seen by wind coming from a certain direction in cm^2. This is to the surface of the obstacle projected on a plane perpendicular to the direction of wind. S is the specific area: if a surface of area A has n roughness elements, $S = A/n$.

More sophisticated formula have been proposed (*Andreas*, 2011) and other metrics exist to find physical roughness and thus compute a preferential orientation (*Nield et al.*, 2013; *Baines and Palmer*, 1990). On complement of these methods, other studies on snow profiles along lines (*Brock et al.*, 2006; *Albert and Hawley*, 2002; *Fassnacht et al.*, 2009) or on elevation maps (*Schirmer and Lehning*, 2011; *Smith et al.*, 2016) have been conducted. We choose Formula (1) because of the simplicity of computations and because aerodynamic roughness can be directly derived. Roughness computations on transects can be implemented, but to study influence of orientation, interpolation on a rotated grid is necessary, which takes too much time compared to implementation of Formula (1).

A script was used to compute s (personal communication, developed by Hervé Bellot [2]), giving some informations about orientation of physical roughness. This is the first step to compute aerodynamic roughness. The choice to spend more time on accumulation processes has been done and thus aerodynamic roughness has not been calculated.

2.4 Accumulation between two scans

The accumulation between two scans is simply one elevation map to which we subtract the previous elevation map. Here the term *accumulation* refers to positive accumulation and to negative accumulation (i.e. erosion). A median filter with 3×3 pixels box size has been applied to remove outliers points.

Duration between two scan is not always one day, due to scanning errors. Following table presents percentage of time duration between two scans for dmc1 and dmc2.

	dmc1	dmc2
1 day	86%	84%
2 days	8%	8%
3 days and more	6%	8%

Circular thin deposit or erosion shapes appear on some accumulation maps. These semi circles are centered on the RLS, indicating that they are not real events but noise occurring during the scanning process. Amplitude of these shapes is usually less than 1 cm.

2.5 Segmentation of patches and derivation of structures orientation

An important part of the positive accumulation is due to well delimited patches. A segmentation processing is used to separate these patches. Segmentation algorithm is a processing tool that

[2] herve.bellot@irstea.fr

works with binary 2D arrays and detects separated regions. The result is a 2D array where each region is labeled with a unique number.

The binary 2D array was computed with a boolean threshold: accumulation $> 1.5\,\text{cm}$. Here the value of 1.5 cm roughly corresponds to the error in the elevation measurement. In addition, a lower value does not allow a good detection of direction of patches and a higher value does not detect small patches. To remove noise on this boolean array an erosion – dilatation morphologic filter with a 5×5 pixels box has been applied.

Once the patches are separated, orientation and elongation of the patches can be computed. The python library *skimage* contains a tool named *measure* [3] that directly gives orientation and elongation of segmented areas. For that, an ellipse that have the same second-moments as the studied area is determined. The orientation is extracted as the orientation of ellipse major axis and eccentricity gives informations about patches elongation. Eccentricity is chosen here as distance between focal points divided by major axis length. As orientation gives an information only on the $[-\pi/2, \pi/2]$ part of the plane, the opposite direction needs to be also plotted on graphs.

We separated accumulation in two terms: one due to patches and the other due to other processes. To compare their effect, total accumulation has been computed for each term. Patches smaller than $0.2\,\text{m}^2$ where removed from the patch term because their detection is over-sensitive to the threshold parameters.

2.6 Computation of deposit age

During my internship only the age since deposition of snow particles, called deposit age. The exposition time of the surface has not been studied, because of lack of time and because time has been spent on accumulation processes. I developed the algorithms to compute the deposit age at one point, and applied it for every point. The principle is to consider a vertical section under the point, corresponding to all the previous accumulation events, each layer contains its deposit age and its vertical position. Few steps are computed to take deposition and erosion into account:

1. create a variable, named *total_ accumulation* and set it to zero;
2. go to next scan;
3. increment by the date difference between actual and previous previous scan every layer deposit age;
4. add the accumulation value to *total_ accumulation*;
5.
   - if *total_ accumulation* $> 1.5\,\text{cm}$: add a new layer to vertical section and put its age to zero;
   - if *total_ accumulation* $< 1.5\,\text{cm}$: remove *total_ accumulation* of snow over new surface and the corresponding layers;
6. go to step 2.

The usage of *total_ accumulation* is necessary to remove noise corresponding to small surface elevation changes. As the precision of the RLS is of the order of the centimeter, when *total_ accumulation* exceeds 1.5 cm in absolute value it very likely corresponds to a real event

[3] https://github.com/scikit-image/scikit-image/blob/master/skimage/measure/_regionprops.py#L350

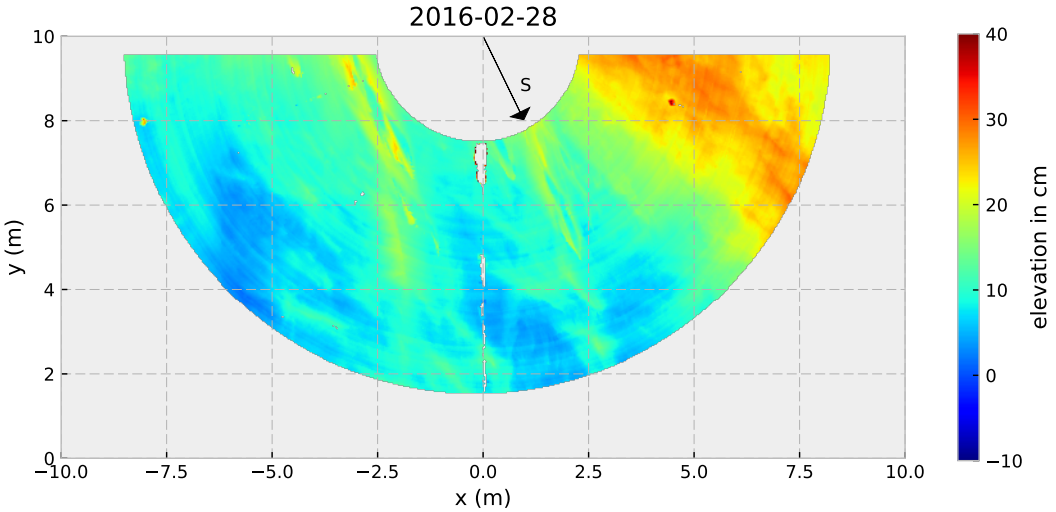

Figure 6: Elevation map of 2016-02-28. The black arrow represents the south direction.

(deposition or erosion). We tried another algorithm where accumulation at the point is used instead of *total_accumulation*, but the part of accumulation which is smaller than the threshold was never taken into account. Thus the described algorithm has been chosen for its more realistic properties. During step 5, when snow has been eroded, surface will reach older snow and age deposit will be older than zero day.

2.7 Wind speed and direction

Genthon et al. (2013) describe measurements from a meteorological mast carrying wind sensors. As the tower may influence the measurement, when the tower is situated between wind origin and instruments, it influences the measurements. The wind speed data have been removed for direction between 50° and 110°. These directions are in minority in the wind rose at Dome C (Figure 3) and thus was not a problem for the analysis of patches. As the meteorological mast does not contain sensors near surface, wind data under 3 m described by *Vignon et al.* (2016) were also used.

3 Results

3.1 Examples of elevation maps

Figure 6 presents the elevation map acquired on 2016-02-28. The mean height is 12.5 cm and the standard deviation 6.3 cm. The mean height is useful to study the temporal evolution. The surface is separated into two rough areas: a high part, situated in the east side, and a low part west. Iso-height lines seem to be oriented along north – south axis, especially for the summit of east part and for green colored level. In addition to this binary division, two sets of elongated dunes are present, one centered around (-2.5 m, 8 m) and the other around (1 m, 7 m). They are composed by few smaller dunes. Both global sets and their smaller size components are oriented along north – south axis. These sets have a metric size along their longest axis and have a decametric size along the small axis. Along the line x = 0 m gray pixels correspond to removed points due to the RLS scanning the shrouds.

Figure 7 presents the elevation map acquired on 2016-03-31. The main structures present

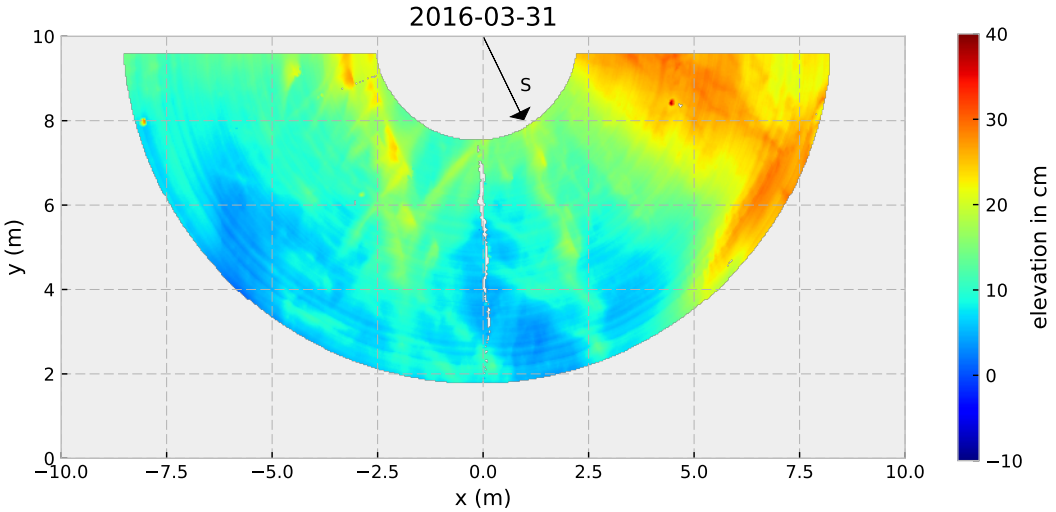

Figure 7: Elevation map of 2016-03-31.

on the elevation map of 2016-02-28 remain in the scan of 2016-03-31. Th map presents two sides with different elevation, two elongated sets of bumps and the shroud effect is visible. The mean surface height is 13.1 cm and the standard deviation is 6.6 cm. Some elongated structures appear around point (1.5 m, 6 m). They are oriented along east-northeast – west-southwest axis and have metric size.

Mean height gives informations on mean accumulation and its temporal evolution. Figure 8 presents a plot of mean height as a function of time. Error bars represent the root mean square (RMS) of surface height, equal here to the standard deviation. The plot has been separated with two different colors because the calculation does not have been executed with the same dataset (*dmc1* or *dmc1*) and thus with different scan sizes. One should take it into account when interpreting the results. The year 2015 presents a big event in July causing an increase of mean height from 0 to 11 cm and of RMS from 4.0 to 6.8 cm. On the contrary the year 2016 underlines an almost constant increase of the mean height, with 9.9 cm of accumulation. RMS increases at one point during the winter and decreases during the rest of time. The slow and gradual evolution of mean height does not represent the surface dynamic.

3.2 Event accumulation

Figure 9 presents two accumulation maps of two successive acquisitions. The two maps show very well separated shapes corresponding to deposition (rose color) or erosion (blue color). Net accumulation is −0.2 cm for 2016-08-12 and standard deviation of accumulation is 2.9 cm; and 0.1 cm for 2016-08-17 with 2.7 cm standard deviation. Net accumulation does not represent the spatial variability of accumulation. An almost zero mean value hides here all the snow displacements. We refer to these deposition shapes as *patches* because each bump corresponds to a particular deposition area. Almost all deposition patches present on map of 2016-08-12 are eroded before the following acquisition, as erosion patterns of 2016-08-17 correspond to these patches. Patches of both scans are approximately oriented along the north – south axis.

For the two scans of 2016-08-12 and 2016-08-17, Figure 10 shows the computed segmented patches. The algorithm selection is satisfying compared to what we see in Figure 9.

From computation of accumulation maps it is possible to compute the positive accumulation, negative accumulation and net accumulation, which simply is the sum of the two precedent terms. Net accumulation is the plotted data on Figure 8. This gives information about snow

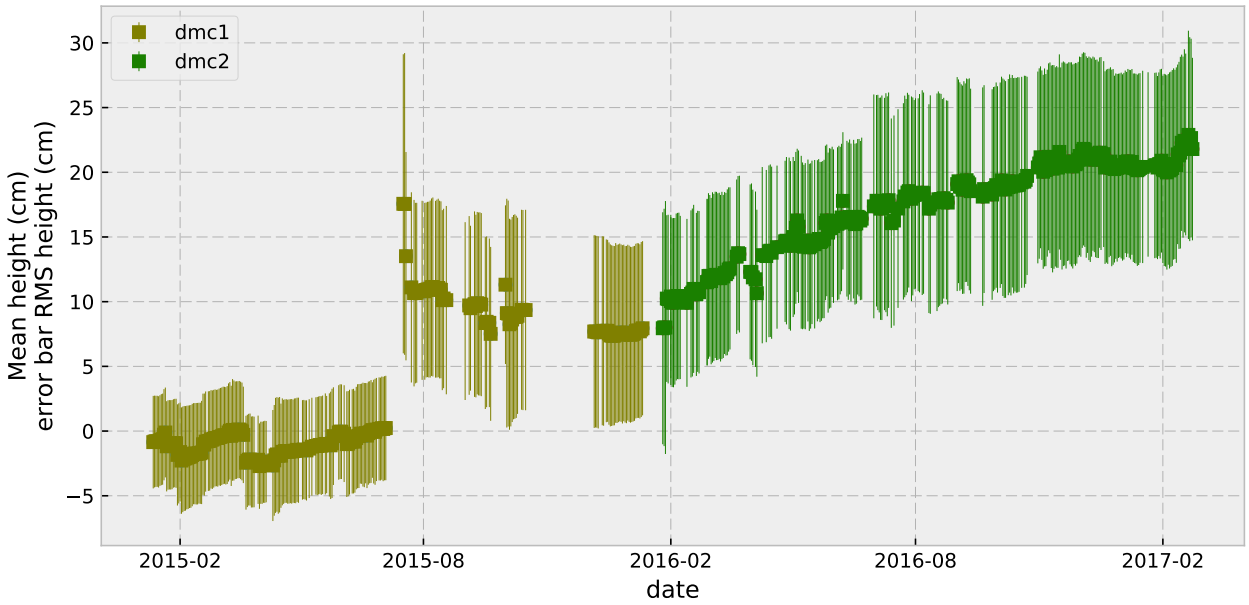

Figure 8: Height and RMS of the surface since installation of the RLS.

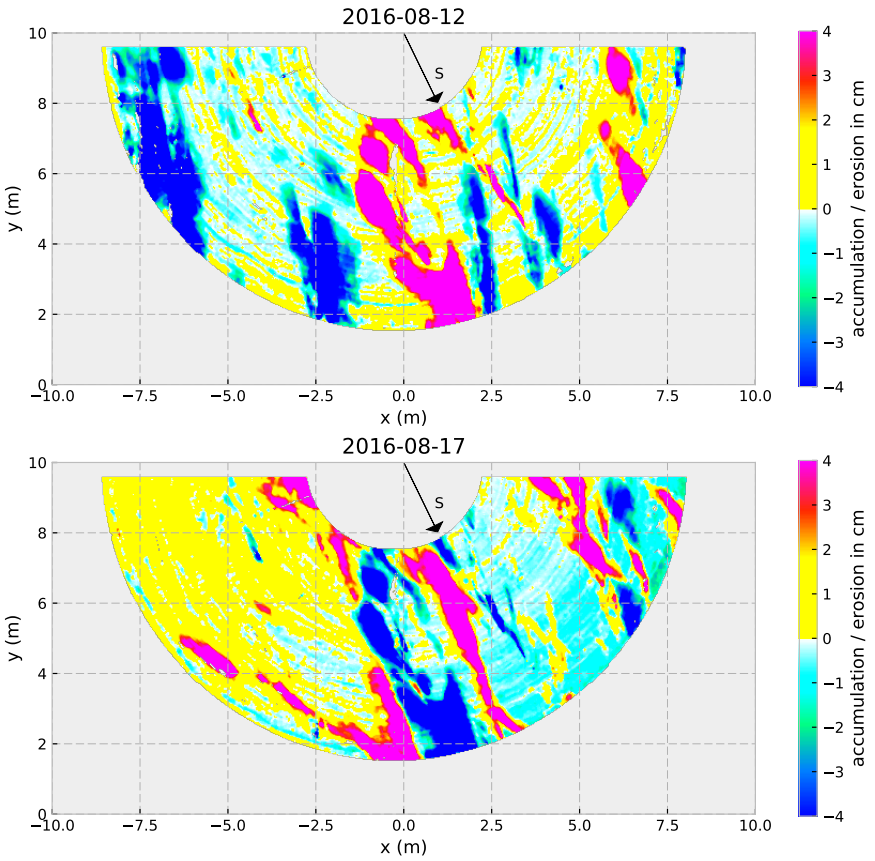

Figure 9: Plots of accumulation for dates 2016-08-12 and 2016-08-17.

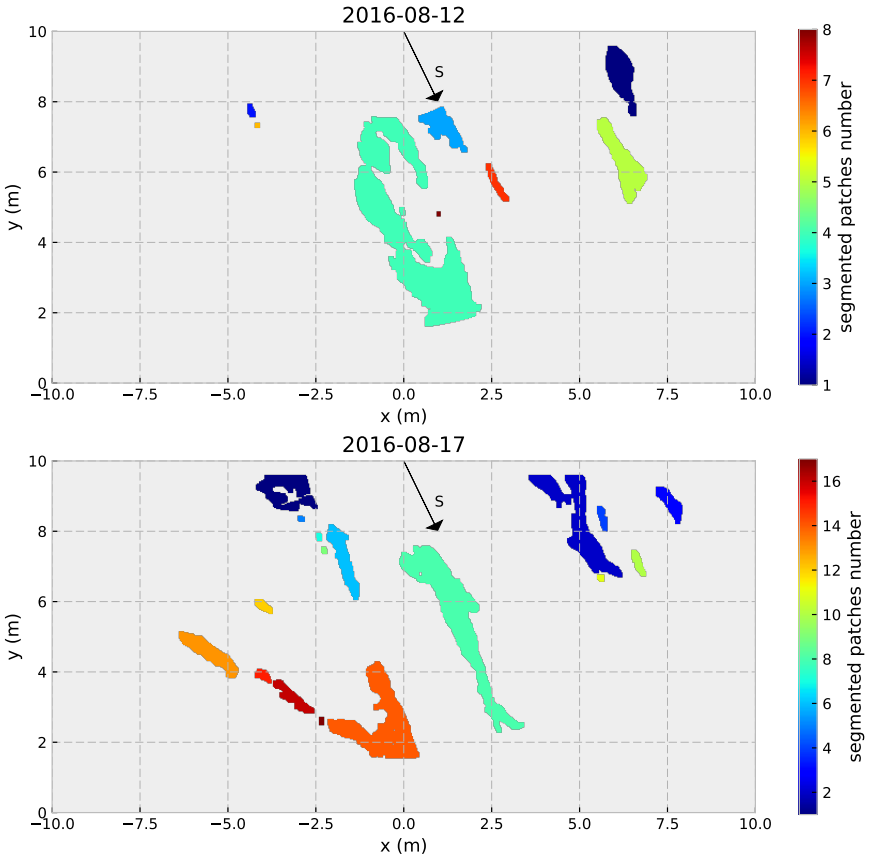

Figure 10: Segmented patches for dates 2016-08-12 and 2016-08-17. Colors correspond to patch number.

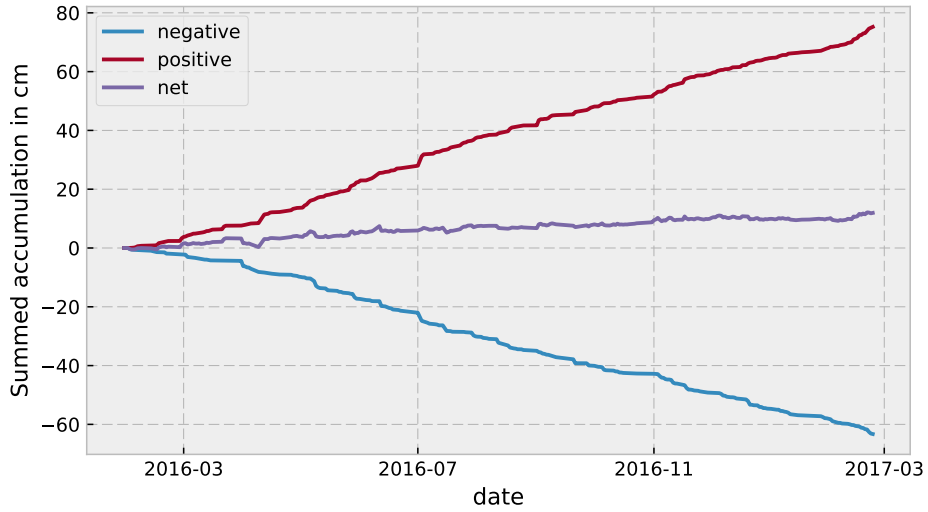

Figure 11: Summed accumulations as a function of time: net elevation, positive gained elevation and cumulated erosion.

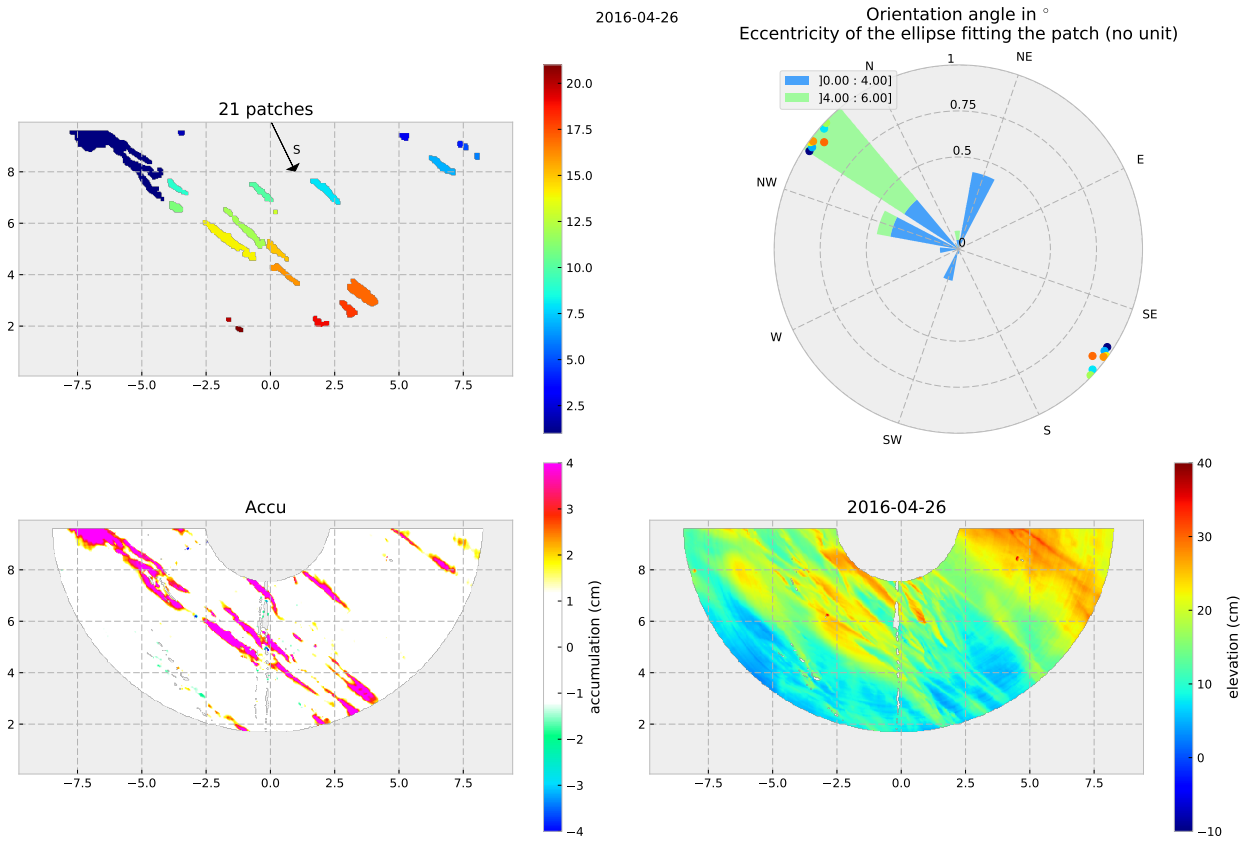

Figure 12: Three maps: the segmented patches, the accumulation and the elevation for 2016-04-26. The wind rose corresponding to wind between the previous scan and this scan is also plotted. It has been rotated to align the north – south axis with the maps one. The bars represent orientation of wind and their color is the wind speed range in $\mathrm{m\,s^{-1}}$. Plotted points represent patches orientation and eccentricity of fitted ellipse. Color of points represent patch number.

transport, as a zero mean can hide a deposition part associated with an erosion one. Figure 11 presents evolution of these three accumulation components, cumulated over time. The purple curve is the net accumulation, equivalent to mean height variations. The red and blue curves are respectively positive and negative cumulated accumulation. The slope of these two curves is almost constant and the positive slope is slightly higher than the negative slope, which yields a positive net accumulation.

Figure 12 presents maps and a wind rose of the direction an the speed of wind since the previous scan. Maps show the orientation of patches. The patches are here very elongated, placed along the pre-existing structures. This event has little erosion component. Points on it are orientation and elongation of patches, obtained by the eccentricity of fitted ellipses. Here the patches are clearly oriented along main wind direction.

Some statistics have been computed on the patches:

- Out of 278 scans acquired for dmc2, 158 do not have patches, 120 feature patches among which 88 have large patches with area $> 0.2\,\mathrm{m}^2$, taken into account in cumulated patch accumulation;
- Among the scans with patches, on average they contain 12.2 patches with a standard deviation of 10.1;

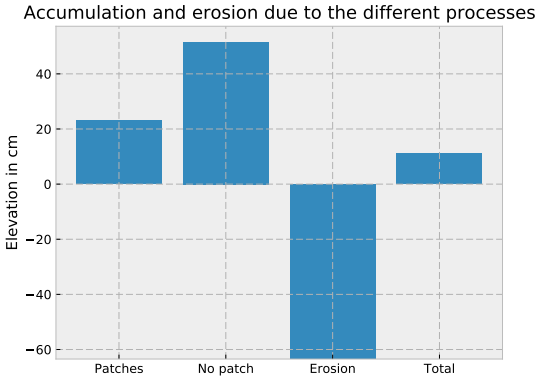

Figure 13: Contribution of large patches (area $> 0.2\,\mathrm{m}^2$), other processes and erosion to total cumulated accumulation for different a segmentation threshold equal to 1.5 cm.

- Among the scans with large patches, on average they contain 3.6 patches with a standard deviation of 3.9.

Figure 13 presents the cumulated accumulation due to big patches, other processes and erosion. 30.8% of total positive accumulation is due to big patches for the 1.5 cm threshold used for computation of their orientation. If a lower threshold is used, the positive accumulation due to patches increases: for a 0.5 cm threshold patches are responsible of around 70% of total positive accumulation.

3.3 Anisotropy of aerodynamic drag

Figure 14 presents the silhouette area of 2016-04-26 elevation map. The effect of north – south oriented elevation structures is visible on the silhouette area plot: they correspond to the two minima. Because of their elongated shapes, surface seen by wind is smaller along principal direction than along perpendicular direction. The silhouette area is about 2 times higher along east – west direction than along north – south direction. At constant obstacle height h^* and specific area S, this creates a variation of the same order of the aerodynamic roughness. This is the origin of a directional anisotropy of the drag.

3.4 Heterogeneous surface deposit age

Deposit age is related to evolution of accumulation. Two different events are presented here: one deposit event and one erosion event. They both influence the deposit age maps with opposite effects.

The studied deposit event occurred between 2016-04-05 and 2016-04-09, without scan between these two dates. Accumulation map of this event together with deposit age maps before and after the event is plotted on Figure 15. Elevation maps of these two days are present in Appendix A, Figure A.1. We observe apparition of big patches oriented along the north – south axis on the accumulation map. On the east side of the scan a more uniform deposit occurs, while erosion occurs on the west side. The 2016-04-05 deposit age map presents distinct zones that have different ages. These zones seem to be superimposed, the older ones under the younger ones. Grey zones are zones where no deposit occurred since the first dmc2 scan or zones that have been eroded beyond the first dmc2 scan: the deposit age is unknown.

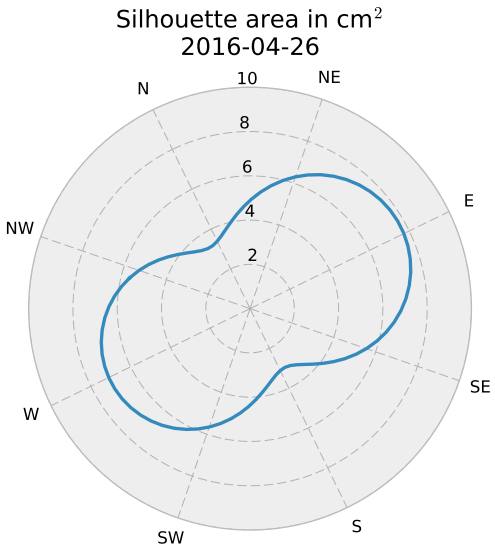

Figure 14: Silhouette area as a function of direction. The north – south orientation of 2016-04-26 elevation map corresponds to minimums in silhouette area. The orientation has been rotated to correspond to the elevation maps orientation.

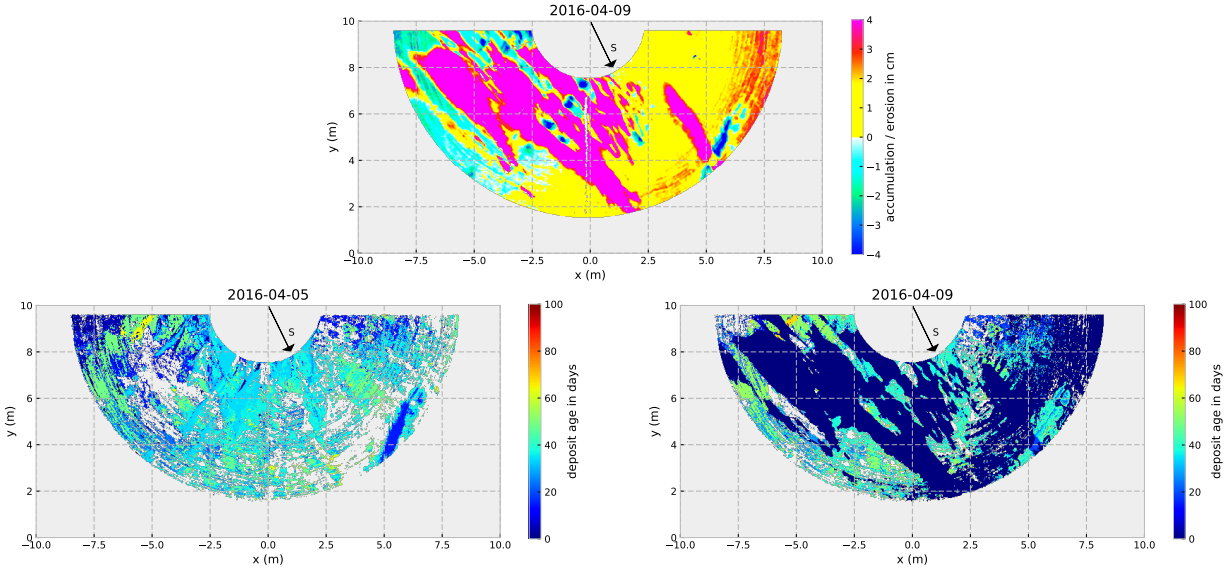

Figure 15: Upper plot is the accumulation map of snow deposited or eroded between 2016-04-05 and 2016-04-09. Below the deposit age maps of 2016-04-05 and 2016-04-09 are represented.

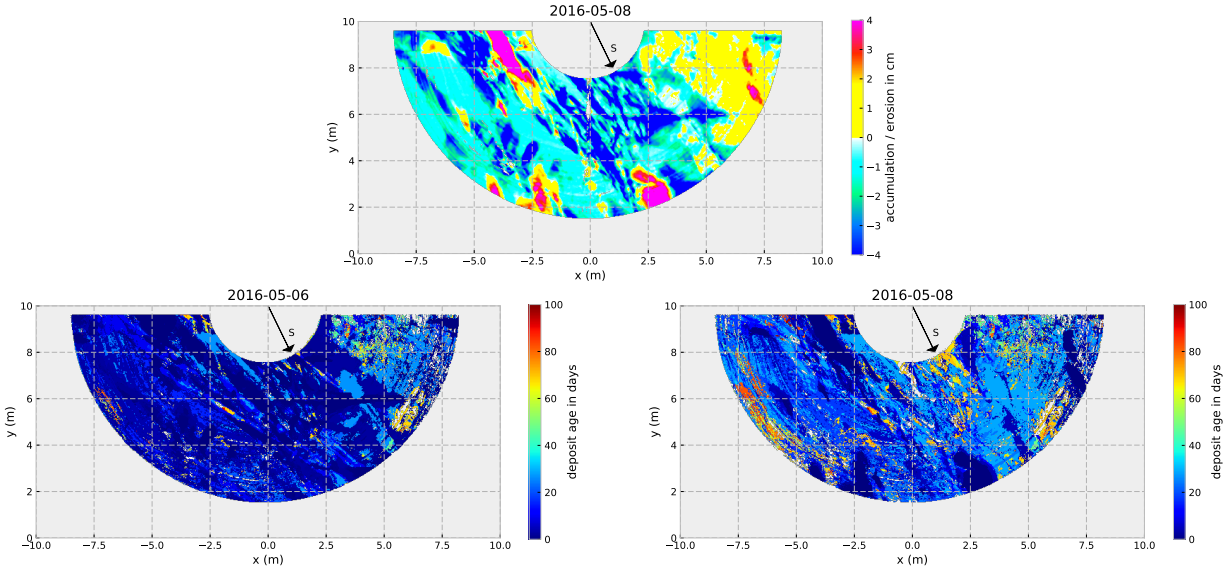

Figure 16: Upper plot is the accumulation map of snow deposited or eroded between 2016-05-06 and 2016-05-08. Below the deposit age maps of 2016-05-06 and 2016-05-08 are represented.

The 2016-04-09 deposit age map contains new snow, dark blue colored, which is distributed following the same shape as accumulation patches. This is coherent with the algorithm used to compute deposit age. New snow is superimposed on the zones present on the 2016-04-09 deposit age map. Deposit events explain the superimposition of homogeneous aged zones: each deposit event adds new patches.

Figure 16 presents an event with a major erosion component. Elevation maps of studied days are present on Appendix A, Figure A.2. Here snow has been eroded, the snow present at the surface after erosion is thus old snow. This is clearly seen around the point (1.5 m, 8 m) where surface snow changes from new snow to snow aged of about 70 days.

The combination of patchy deposition and erosion yield heterogeneous surface in terms of deposit age. Figure 17 shows an example of heterogeneous surface. New snow patches lie near snow older than 90 days. Many patches that have same ages are visible, corresponding to deposit events with patches.

4 Discussion

The RLS is a robust instrument that provides near daily elevation maps. In spite of the failures that occur during drifting events, interesting and innovative results have been found by an analysis of these maps.

Two years of data are available, 2015 named dmc1 and 2016 named dmc2. Between these two years, the RLS have been risen up to scan a bigger area, thereby it is not directly possible to study the whole dataset as one. Between the two years, mean elevation featured two very different trends. While mean elevation was almost constant excepted during one big event for dmc1, mean elevation presents an almost constant increase for dmc2. The surface is different between these two datasets but *Picard et al.* (2016) showed that surface of dmc1 dataset had the same yearly mean behavior as a kilometric surface. This indicates that the surface representativity was equivalent to a larger surface. Good confidence is placed on the fact that the differences between dmc1 and dmc2 are caused by temporal variations and not by spatial dependence. This question can not been elucidated yet with RLS data as it has been

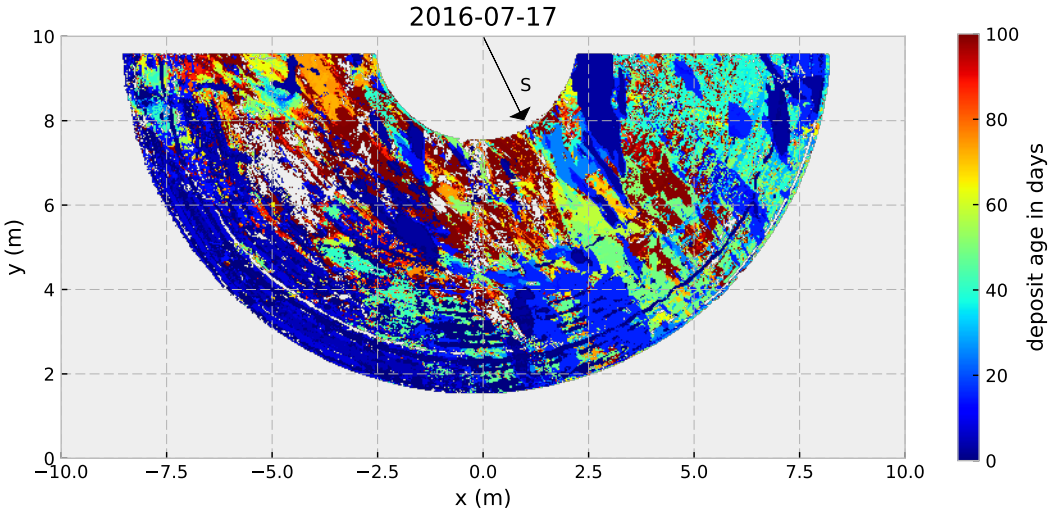

Figure 17: Heterogeneity of deposit age on the surface: example of 2016-07-17.

working for a too short time. In addition, even if surface yearly mean elevation is consistent with wider surfaces, this does not mean that the disposition of patches is representative, the RLS can influence the wind flow around the scanned surface and thus influence the accumulation processes. Presence of the big bump on east side of elevation maps could be partially influence by buildings artificial relief of scientific equipment.

Figure 13 presents the contribution of patches to global positive accumulation. The method used to compute this value is simple as it sums deposit of every patch, which gives information about quantity of patches that appear. Nevertheless this does not give information about the quantity of added snow by patches that is permanent. The heterogeneous look of deposit age maps (Figure 17) provides a clue that the contribution of patches to permanent snow deposit is not negligible and maybe major, but the erosion needs to be more precisely studied to solve this question.

During the segmentation process a threshold has been used: the minimum deposit to be considered as a patch. The 1.5 cm value has been chosen based on RLS precision argument and efficiency argument for orientation computation. A different threshold leads to different values of accumulation due to patches and the question of its value is open. Another threshold also leads to different statistics about patches (percentage with patches, number of patches, etc). During my internship, only one threshold was used for patches orientation, patches accumulation and deposit age computations. Age computation is less sensitive to the value of the threshold as little fluctuations of elevation are compensating. To calculate the orientation of a patch it is necessary to take its summit part into account to be more precise, but the whole patch is important for net accumulation.

Deposit age maps alone provide informations about deposit and erosion of snow. Associated with elevation maps and accumulation maps it is possible to describe history of the surface, but results have to be studied with attention. As deposit age is computed with the use of a threshold, small events can be undetected. These small events can partially cover the surface and thus influence snow exposition time. The exposition time of snow grains on the surface influences metamorphism processes, albedo, and snow – air exchanges. Deposit age maps and accumulation maps are not sufficient to access to this quantity. This was not the subject of this study and the deposit age provided enough informations about accumulation patchy shape.

Despite these questions it seems clear that mean elevation is not sufficient to describe

surface evolution. Further work on RLS data is necessary to clarify some points, but net accumulation must be considered with precaution in the Antarctica Plateau as it does not represent the complexity of surface changing leading to very heterogeneous surface age.

5 Conclusion

Climate of Antarctica is crucial in the global Earth climate, including katabatic wind speed over Antarctica, sea-ice formation, and ocean-bottom water formation (*King et al.*, 2001), all influenced by snow surface heat flux. Aerodynamic parameters that control this flux are influenced by surface shapes, especially sastrugi (*Jackson and Carroll*, 1978; *Vignon et al.*, 2016). Understanding deposit and erosion processes is necessary to better constraint models inputs and thus to improve predictions.

During my internship I studied elevation maps acquired by a RLS placed at Dome C since 2015. Accumulation maps have been processed by substracting one map by the previous one. With only few centimeter of snow accumulation per year, Dome C presents a completely different behavior from the Alpine one, where a snowfall usually deposes a decimetric snow layer. Between two consecutive days, net accumulation is near zero but surface undergoes a lot of erosion and deposit with snow drift. Both processes are almost compensating themselves. Accumulation is not uniform on surface and 30 to 70% of the positive accumulation, depending on detection threshold, is due to patches. These patches are well separates each from others and thus can be detected with segmentation analyzes. Some events present very elongated patches oriented along wind direction. This behavior is not systematic and no evidence effect of wind speed has been shown.

We developed an algorithm to compute the surface deposit age. In agreement with accumulation results, during accumulation events surface deposit age is reset to zero mainly where patches appear. As a result the surface deposit age is very heterogeneous, age differences between two points can exceed 100 days, which influences snow – air exchanges and metamorphism of snow. The surface must not be considered as uniform for the study of these questions.

Further work is necessary to complete the analyses of this report. As only two year of elevation maps are available, time representativity of the studied processes is not well established. Patches play a non negligible role on everyday deposit and on durable deposit, that is seen on accumulation statistics and on deposit age maps where old patches are visible. No statistical analyzes has been done yet to characterize how much of them are eroded or durable. Moreover their apparition and position are not characterize now.

The RLS present at Dome C allows a precise study of aerodynamic properties of surface and snow accumulation processes. Its new kind of data allow a new characterization of Antarctica surface. This will have influence on models that predict future but also on reconstruction of past climate.

References

Albert, M. R., and R. L. Hawley (2002), Seasonal changes in snow surface roughness characteristics at summit, greenland: implications for snow and firn ventilation, *Annals of Glaciology*, *35*(1), 510–514.

Amory, C., F. Naaim-Bouvet, H. Gallée, and E. Vignon (2016), Brief communication: Two well-marked cases of aerodynamic adjustment of sastrugi, *The Cryosphere*, *10*(2), 743–750, doi:10.5194/tc-10-743-2016.

Andreas, E. L. (2011), A relationship between the aerodynamic and physical roughness of winter sea ice, *Quarterly Journal of the Royal Meteorological Society*, *137*(659), 1581–1588.

Baines, P. G., and T. Palmer (1990), *Rationale for a new physically-based parametrization of subgridscale orographic effects*, ECMWF Shinfield Park, Reading, Berkshire RG2 9AU, UK.

Brock, B. W., I. C. Willis, and M. J. Sharp (2006), Measurement and parameterization of aerodynamic roughness length variations at haut glacier d'arolla, switzerland, *Journal of Glaciology*, *52*(177), 281–297.

Brun, E., D. Six, G. Picard, V. Vionnet, L. Arnaud, E. Bazile, A. Boone, A. Bouchard, C. Genthon, V. Guidard, et al. (2011), Snow/atmosphere coupled simulation at dome c, antarctica, *Journal of Glaciology*, *57*(204), 721–736.

Champollion, N., G. Picard, L. Arnaud, E. Lefebvre, and M. Fily (2013), Hoar crystal development and disappearance at dome c, Antarctica: observation by near-infrared photography and passive microwave satellite, *The Cryosphere*, *7*(4), 1247–1262, doi:10.5194/tc-7-1247-2013.

Ding, M., T. Zhang, C. Xiao, C. Li, B. Jin, L. Bian, S. Wang, D. Zhang, and D. Qin (2017), Snowdrift effect on snow deposition: Insights from a comparison of a snow pit profile and meteorological observations in east antarctica, *Science China Earth Sciences*, *60*(4), 672–685.

Fassnacht, S. R., M. Williams, and M. Corrao (2009), Changes in the surface roughness of snow from millimetre to metre scales, *Ecological Complexity*, *6*(3), 221–229.

Filhol, S., and M. Sturm (2015), Snow bedforms: A review, new data, and a formation model, *Journal of Geophysical Research: Earth Surface*, *120*(9), 1645–1669.

Genthon, C., D. Six, H. Gallée, P. Grigioni, and A. Pellegrini (2013), Two years of atmospheric boundary layer observations on a 45-m tower at dome c on the antarctic plateau, *Journal of Geophysical Research: Atmospheres*, *118*(8), 3218–3232, doi:10.1002/jgrd.50128.

Groot Zwaaftink, C., A. Cagnati, A. Crepaz, C. Fierz, G. Macelloni, M. Valt, and M. Lehning (2013), Event-driven deposition of snow on the antarctic plateau: analyzing field measurements with snowpack, *The Cryosphere*, *7*(1), 333–347.

Jackson, B. S., and J. J. Carroll (1978), Aerodynamic roughness as a function of wind direction over asymmetric surface elements, *Boundary-Layer Meteorology*, *14*(3), 323–330, doi:10.1007/BF00121042.

Kaasalainen, S., H. Kaartinen, A. Kukko, K. Anttila, and A. Krooks (2011), Brief communication" application of mobile laser scanning in snow cover profiling", *The Cryosphere*, *5*(1), 135.

King, J., W. Connolley, and S. Derbyshire (2001), Sensitivity of modelled antarctic climate to surface and boundary-layer flux parametrizations, *Quarterly Journal of the Royal Meteorological Society*, *127*(573), 779–794.

Kukko, A., K. Anttila, T. Manninen, S. Kaasalainen, and H. Kaartinen (2013), Snow surface roughness from mobile laser scanning data, *Cold Regions Science and Technology*, *96*, 23–35.

Lacroix, P., B. Legrésy, K. Langley, S. Hamran, J. Kohler, S. Roques, F. Rémy, and M. Dechambre (2008), Instruments and methods in situ measurements of snow surface roughness using a laser profiler, *Journal of Glaciology*, *54*(187), 753–762.

Lettau, H. (1969), Note on aerodynamic roughness-parameter estimation on the basis of roughness-element description, *Journal of applied meteorology*, *8*(5), 828–832.

Libois, Q., G. Picard, L. Arnaud, S. Morin, and E. Brun (2014), Modeling the impact of snow drift on the decameter-scale variability of snow properties on the antarctic plateau, *Journal of Geophysical Research: Atmospheres*, *119*(20), 11,662–11,681, doi:10.1002/2014jd022361.

Nield, J. M., J. King, G. F. Wiggs, J. Leyland, R. G. Bryant, R. C. Chiverrell, S. E. Darby, F. D. Eckardt, D. S. Thomas, L. H. Vircavs, et al. (2013), Estimating aerodynamic roughness over complex surface terrain, *Journal of Geophysical Research: Atmospheres*, *118*(23).

Picard, G., F. Domine, G. Krinner, L. Arnaud, and E. Lefebvre (2012), Inhibition of the positive snow-albedo feedback by precipitation in interior antarctica, *Nature Climate Change*, *2*(11), 795–798.

Picard, G., L. Arnaud, J.-M. Panel, and S. Morin (2016), Design of a scanning laser meter for monitoring the spatio-temporal evolution of snow depth and its application in the alps and in Antarctica, *The Cryosphere*, *10*(4), 1495–1511, doi:10.5194/tc-10-1495-2016.

Schirmer, M., and M. Lehning (2011), Persistence in intra-annual snow depth distribution: 2. fractal analysis of snow depth development, *Water Resources Research*, *47*(9).

Schirmer, M., V. Wirz, A. Clifton, and M. Lehning (2011), Persistence in intra-annual snow depth distribution: 1. measurements and topographic control, *Water Resources Research*, *47*(9).

Shepherd, A., and D. Wingham (2007), Recent sea-level contributions of the antarctic and greenland ice sheets, *science*, *315*(5818), 1529–1532.

Smith, M. W., D. J. Quincey, T. Dixon, R. G. Bingham, J. L. Carrivick, T. D. Irvine-Fynn, and D. M. Rippin (2016), Aerodynamic roughness of glacial ice surfaces derived from high-resolution topographic data, *Journal of Geophysical Research: Earth Surface*, *121*(4), 748–766.

Vignon, E., C. Genthon, H. Barral, C. Amory, G. Picard, H. Gallée, G. Casasanta, and S. Argentini (2016), Momentum- and heat-flux parametrization at dome c, Antarctica: A sensitivity study, *Boundary-Layer Meteorology*, *162*(2), 341–367, doi:10.1007/s10546-016-0192-3.

Zhuravleva, T. B., and A. A. Kokhanovsky (2011), Influence of surface roughness on the reflective properties of snow, *Journal of Quantitative Spectroscopy and Radiative Transfer*, *112*(8), 1353–1368.

A Results

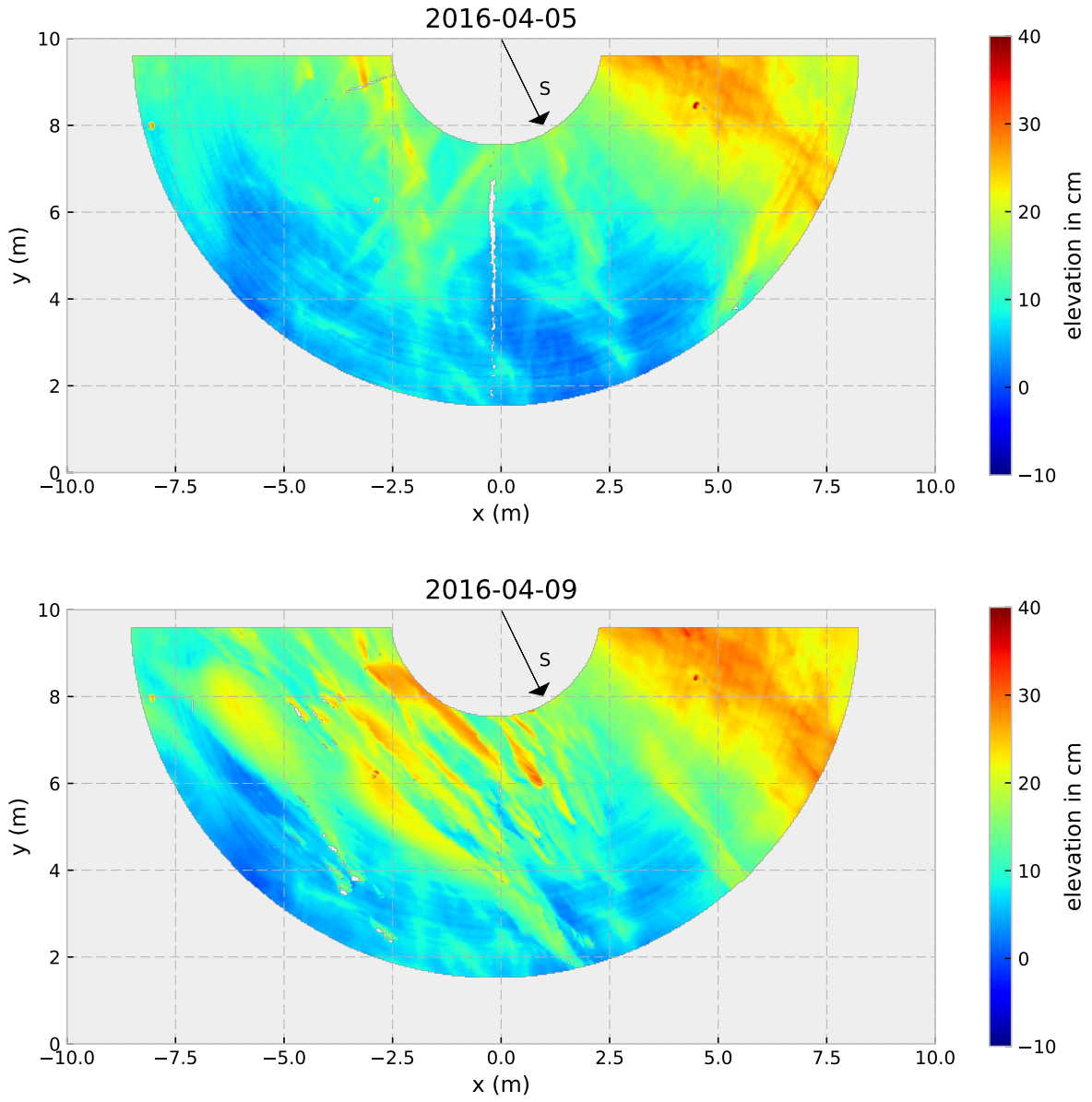

Figure A.1: Elevation maps of the accumulation event studied in Section 3.4

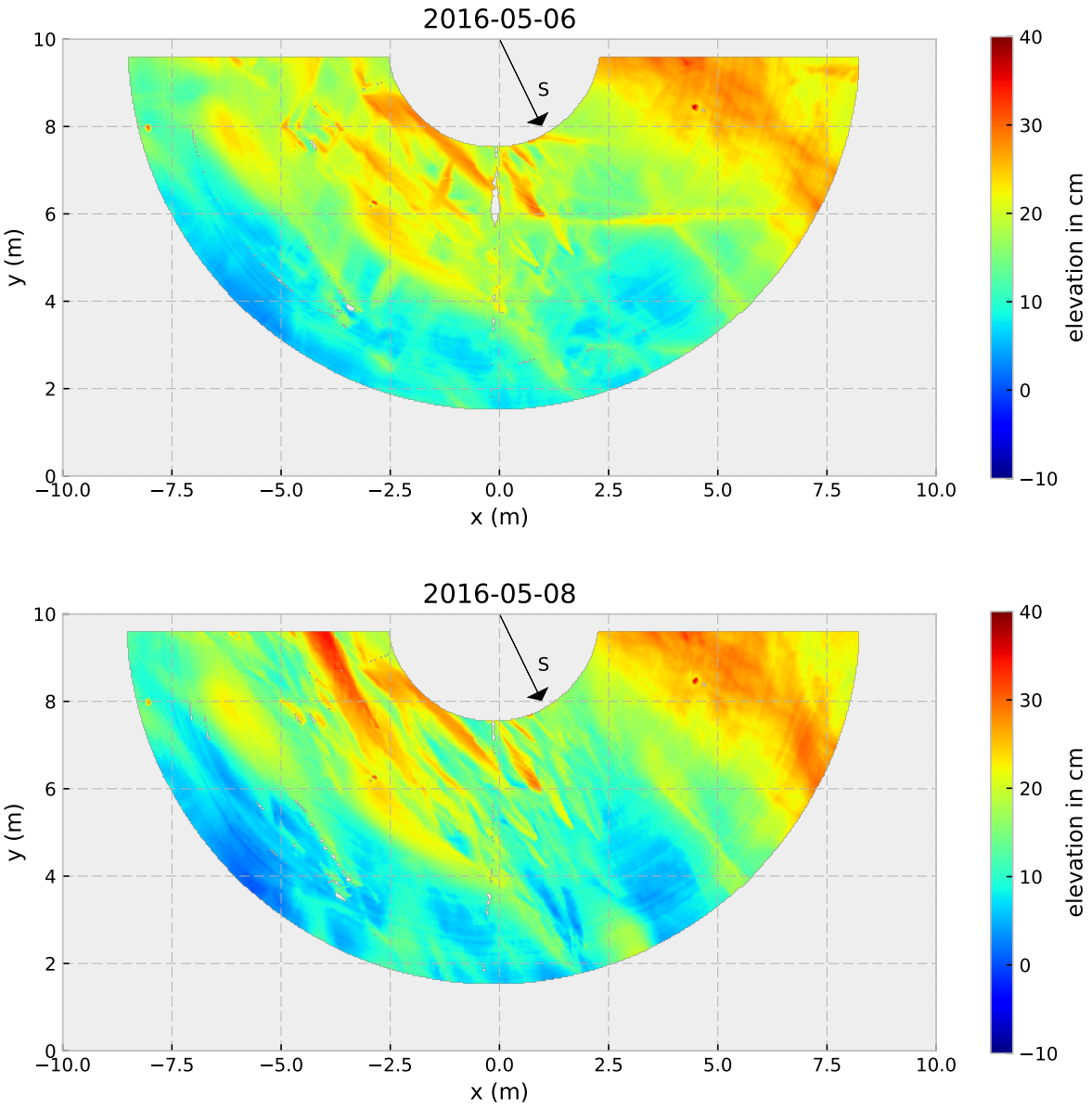

Figure A.2: Elevation maps of the erosion event studied in Section 3.4